Flowfield Experiments on a DF Chemical Laser

Richard J. Driscoll* and George W. Tregay†
Bell Aerospace Textron, Buffalo, New York

Diagnostic experiments were conducted on a DF chemical laser to obtain data on the reaction zone structure for laminar mixing and when the mixing has been augmented by gas jet injection at the reactant interface. DF and HF emission from the reaction zones was recorded using infrared sensitive film and an IR scanner with an InSb detector; DF small-signal gain experiments were also conducted. The IR scanner and gain measurements were used to verify the photographic data which showed a decrease in the axial mixing length from 5 cm to 0.5-1.0 cm in going from the laminar to the augmented mixing mode.

Introduction

In a continuous wave DF chemical laser, reactants enter the laser cavity through separate supersonic nozzles as is shown in Fig. 1. The atomic fluorine (F) and deuterium (D_2) mix and then react via the cold reaction $F + D_2 \rightarrow DF(v) + D$, $v = 1\text{-}4$, to produce vibrationally excited DF. Energy is extracted as laser radiation from the inverted $DF(v)$ population using a suitable optical resonator.

The chemical efficiency η_c for this type of laser has a strong dependence on the reactant mixing rate.[1,2] As the mixing rate becomes faster, η_c increases until the premixed limit is reached. When operated in the laminar mixing mode, η_c varies with cavity pressure p as $\eta_c \sim 1/p$, reflecting the inverse pressure dependence of the molecular diffusivity. While η_c decreases with increasing pressure, the pressure recovery potential of the flow increases with pressure.[3] When high pressure recovery is an essential requirement, the simultaneous achievement of a high laser efficiency can only be obtained using nozzle designs which yield mixing rates faster than those achievable in the laminar mode. It was to satisfy the joint requirements of high efficiency and pressure recovery that the so-called "trip" nozzle was developed.

The trip nozzle shown in Fig. 1 uses helium gas jets located at the end of the nozzle blades at the reactant interface to disturb the flow such that the reactant mixing rate increases. Witte et al.[4] were the first to demonstrate this technique and they showed that the gas jet injection increased the excited specie production rate by factors from 2 to 3. Cummings et al.[5] showed that the gas jets increased the power output of their laser by about 60%, while Wilson and Hook[6] reported an 80% power increase due to the faster mixing.

The mechanism by which the gas jets increase the mixing rate is not well understood. Since the nozzle shear layers become turbulent naturally,[7] it is sometimes assumed that the gas jets accelerate the laminar-to-turbulent flow transition. The nonreacting flow measurements of Cenkner[8] show, however, that the jets do not increase the turbulence level of the flow, therefore implying that there is no basis for using turbulence as an explanation for the faster mixing. Thus, the commonly used terms "trip nozzle" and "trip jet" are probably misnomers in the sense that they imply a transitional or turbulent mixing mechanism. In fact, the recent nonreacting flow visualization studies of Cenkner and Driscoll[9] suggest another mechanism based on the jets distorting the reactant interface so as to increase the contact area between the reactant streams. Flow and laser performance models based on this reactant-surface stretching mechanism have recently been developed by Driscoll[10] and it is found that these models can provide a qualitative explanation for the faster mixing and increased laser performance obtained from these lasers.

An understanding of the gas jet mixing mechanism is essential if one is to develop models which can accurately predict the media gain distributions for the different lasing lines. Such information is needed to design the optical resonators[11] which extract the power from the flow. Current models[11,12] are empirical in nature and either specify the diffusion coefficient or the mixing zone boundaries so as to achieve agreement with gain data. They do not attempt to model a physical mixing mechanism as does the more recent model proposed by Driscoll.[10] The shortcomings of earlier models can be traced, in part, to the lack of reacting flow data against which such models can be tested. In this paper, we present photographic data for a DF laser operating in both the laminar and augmented mixing mode. These data provide a clear demonstration of the change in the reaction characteristics due to the gas jets and also illustrate the utility of photographic information as a diagnostic tool. In addition, data on the axial and cross-nozzle small-signal gain distributions and emission profiles from an infrared scanner are presented in order to verify the photographic results and also to provide quantitative data for the testing of flow models.

Flowfield Experiments

All of the experiments to be described herein used the CL-XI nozzle array operating as a DF laser. The laser was operated using C_2H_4 and NF_3 as the combustor fuel and oxidizer; helium was the combustor diluent. The combustor is run oxidizer-rich at 1700 K to produce atomic fluorine. For these tests, the laser fuel was deuterium (D_2) with the laser fuel stream diluent being helium. The nominal operating condition is a nozzle mass flux ($\dot{m}/A$) of 2.0 g/s-cm^2, where $\dot{m}$ is the total laser mass flow (primary, secondary, and trip) and A is the active frontal area of the nozzle array; tests were also conducted at $\dot{m}/A = 1.5$ and 2.5 g/s-cm^2. Diluent and mixture ratios were set at levels which had the optimum closed cavity power during previous experiments. During the experiments, tests were conducted at various gas jet flowrates and with the cavity fuel (D_2) both on and off in order to define the effect of trip flow and cavity heat release on the reactant mixing rates.

A picture of the nozzle array and laser cavity is shown in Fig. 2. The overall size of the nozzle array is 3.5×10 cm. The laser cavity flow is totally enclosed by sidewalls which diverge

Presented as Paper 81-1271 at the AIAA 14th Fluid and Plasma Dynamics Conference, Palo Alto, Calif., June 23-25, 1981; submitted July 16, 1981; revision received May 13, 1982.

*Group Leader, Laser Fluid Mechanics. Member AIAA.
†Staff Scientist, High Energy Laser Technology. Member AIAA.

at 9 deg and horizontal top and bottom walls. This cavity ducts the flow into the supersonic diffuser located downstream of the laser cavity and from there, into the vacuum system. This cavity was designed to duplicate as closely as possible the cavity design used during laser power experiments. As shown in Fig. 2, the laser cavity sidewalls have window apertures on both sides, centered on the nozzle. The window apertures are 2.5 cm wide and extend 5 cm downstream from the nozzle face; sapphire windows were used during these experiments. The width of the windows is such that six of the primary (oxidizer) nozzles and seven of the secondary (fuel) nozzles can be observed. All photographs were taken using a motorized Nikon 35-mm camera with a 135-mm lens. Photographs of the infrared emission from the cavity flow were made using Kodak High Speed Infrared Film (HIE-135). This film is sensitive to infrared radiation at wavelengths of 1.0 μm or less. Best results were obtained with the HIE-135 film with the camera set in the range of f5.6-8 using a 5-10 s exposure.

Measurements of the spontaneous emission from the cavity flow were made using a Dynard Series 210 Thermal Imaging System (IR scanner). The scanner was used with an auxiliary telescope focused on the laser cavity window aperture. The 100 scan lines of the instrument were distributed over a 4.5 cm field of view yielding a 22 lines/cm resolution in the axial flow direction. The scanner was used with a LN_2-cooled InSb detector which is sensitive to radiation in the 2-5 μm wavelength region.

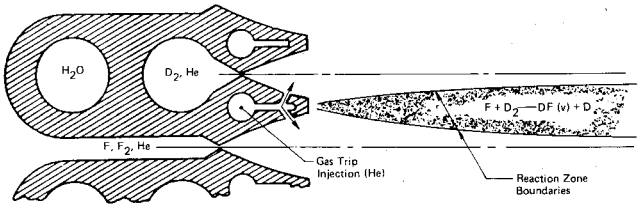

Fig. 1 CL-XI nozzle and flowfield.

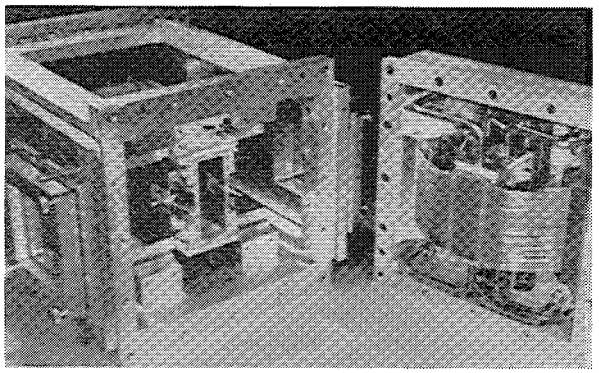

Fig. 2 CL-XI experimental configuration.

Two types of small signal gain measurements will be presented, the first being cross-nozzle gain distributions at various axial stations, the second, axial distributions of the average gain in the cross-nozzle plane. The cross-nozzle gain measurements were made in the cavity shown in Fig. 2; the axial distributions were measured in the power test cavity configuration.

Photographic Tests

Figure 3 shows a typical result from the photographic tests recording DF infrared emission. The test condition is for $\dot{m}/A = 1.5$ g/s-cm^2 and $\mu = 4.0\%$, where μ = jet mass flowrate/total mass flowrate. As indicated, there is relatively little recorded emission in the first 2 cm downstream of the nozzle. Exposure times as long as 10 s were used; however, the long exposure time did not improve the results. It was found that photographs of DF IR emission were of little value in defining the near-nozzle reactant mixing zones, and it was concluded that IR photography of DF cavity emission is not a useful diagnostic technique for studying reactant mixing.

Under similar conditions, HF emission is much stronger than DF emission. Thus the possibility exists that the mixing zones in the flow could be made visible by seeding the fuel stream with a small amount of H_2. The amount of H_2 introduced into the cavity flow should be small compared to the cavity fuel (D_2) flowrate so as not to change the dynamics of the cavity flow as determined by $F + D_2$ reaction rate.

To determine if the H_2 seeding concept had merit, tests were conducted in which a small amount of H_2 (0.10 g/s) was added to the secondary fuel streams. Figure 4 shows the result from one of these tests at the $\dot{m}/A = 1.5$ g/s-cm^2, $\mu = 2.0\%$ condition. It is apparent that the H_2 seeding technique enhances the visibility of the reaction zones in the near nozzle region when compared to the results in Fig. 3.

Zones of HF emission imply the presence of both H_2 and atomic fluorine. The near IR emission ($\lambda \leq 1$ μm) which is recorded results when HF is pumped into the upper ($v \geq 3$) vibrational levels by the cold reaction, $H_2 + F \rightarrow HF(v) + H$, and subsequent v-v transfer reactions, and decays spontaneously by $\Delta v \geq 3$ transitions. Thus HF emission in a spatial region requires the simultaneous presence of H_2 from the secondary stream and F from the primary stream, thereby implying that the primary and secondary streams are mixed on some scale at that point.

The results in Fig. 4 indicate that at the 2% jet flow level, the primary stream becomes mixed at about 1.5 cm from the nozzle. The mixing length is defined as the axial location at which emission occurs on the stream centerline. Using this definition, it is not clear that the secondary stream is ever fully mixed within the 5 cm field of view. Figure 5 shows the same test condition as that of Fig. 4 except that the jet flow level is 6%. Increasing the jet flowrate to the 4% and greater level decreases the secondary mixing length from the indeterminant level indicated in Fig. 4 to about 0.50 cm. The primary stream mixing length also decreases as the jet flow level increases;

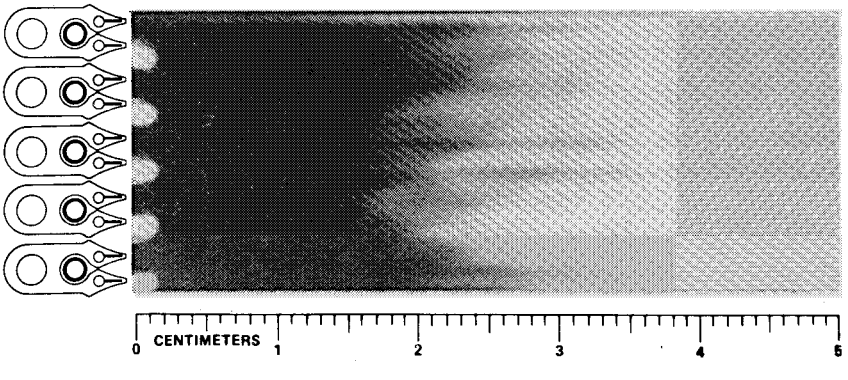

Fig. 3 DF cavity emission, $\mu = 4\%$.

however, the change is less than that for the secondary and the photographs indicate an asymptotic length of about 1 cm.

Table 1 gives a summary of the primary and secondary mixing lengths for the $\dot{m}/A = 1.5$, 2.0, and 2.5 g/s-cm^2 tests over the jet flow range at which tests were conducted. Since the values of the mixing length given are based on a subjective interpretation of the photographic records, the numbers are viewed as representative with little significance being attached to 0.1 cm differences. The results of Table 1 indicate for jet flows of 4% and above, the primary and secondary mixing lengths are about 1.0 and 0.5 cm, respectively, more or less independent of jet flow and mass throughout. At the lower 2-2.5% jet flow levels, the mixing lengths are somewhat longer, with the secondary flow mixing length showing more sensitivity to the jet flow than the primary mixing length.

Figure 6 shows the result when the cavity D_2 has been turned off, i.e., when there is no heat release in the flow except that associated with the 0.1 g/s of H_2; this is quite small (down by approximately a factor of 50 from the normal heat release level). It is seen that the primary flow mixing length is approximately 1 cm, the same as that in Fig. 5, where the heat release is at the nominal level. The secondary flow mixing length is approximately 0.5 cm in Fig. 6 for the no-heat release condition and is somewhat longer, about 0.8 cm, for the flow with the nominal heat release. We conclude from these results, and similar results for the $\dot{m}/A = 2.0$ and 2.5 g/s tests, that the cavity heat release level does not have a first-order influence on the reactant mixing rates in the near-nozzle region.

It is noted that the photographs taken with the cavity fuel off exhibited brighter and more uniform emission zones than the corresponding picture with the D_2 on. The increased photographic clarity is believed due to the fact that, with the D_2 off, the small amount of H_2 present does not have to

Table 1 Primary and secondary nozzle mixing lengths as a function of mass flux and trip flow rate

	Mixing lengths, cm	
	Primary	Secondary
$\dot{m}/A = 1.5$		
$\mu = 2.0\%$	1.50	...
$\mu = 4.0\%$	1.00	0.60
$\mu = 6.0\%$	0.95	0.40
$\dot{m}/A = 2.0$		
$\mu = 2.5\%$	1.20	0.80
$\mu = 3.9\%$	1.00	0.65
$\mu = 5.0\%$	0.85	0.45
$\dot{m}/A = 2.5$		
$\mu = 2.5\%$	1.10	0.90
$\mu = 5.0\%$	1.00	0.50
$\mu = 7.0\%$	0.90	0.45

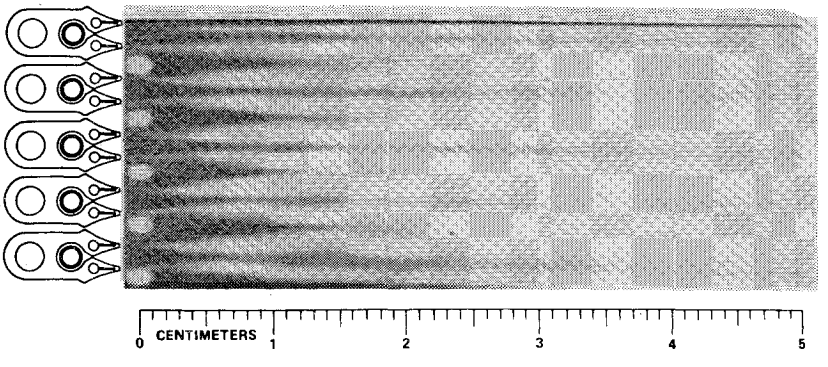

Fig. 4 HF cavity emission, $\mu = 2\%$ (0.10 g/s H_2 in secondary).

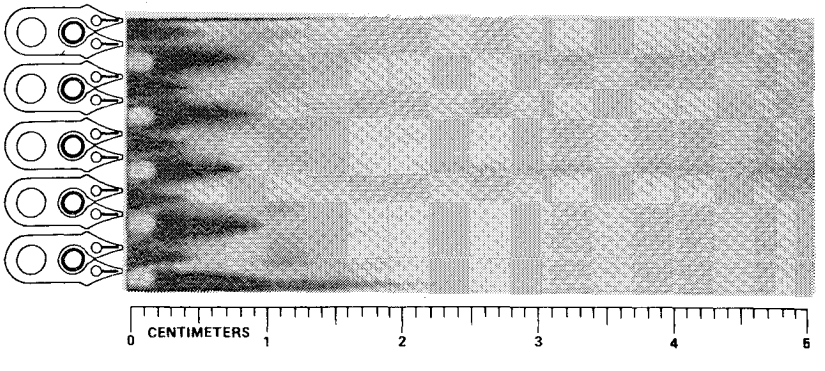

Fig. 5 HF cavity emission, $\mu = 6\%$ (0.10 g/s H_2 in secondary).

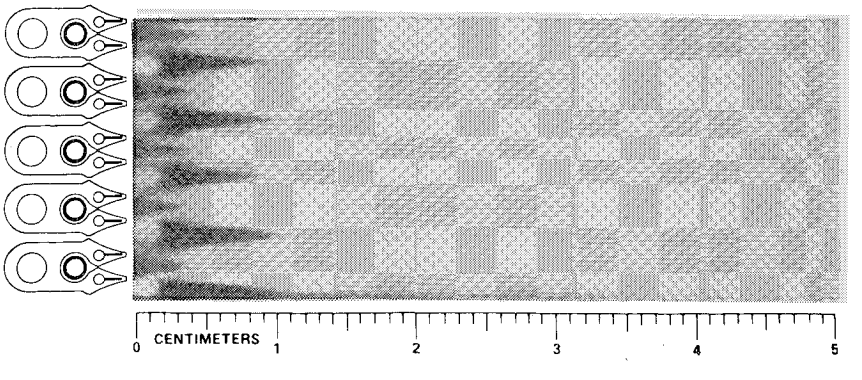

Fig. 6 HF cavity emission, $\mu = 4\%$ [0.10 g/s H_2 in secondary, cavity fuel (D_2) off].

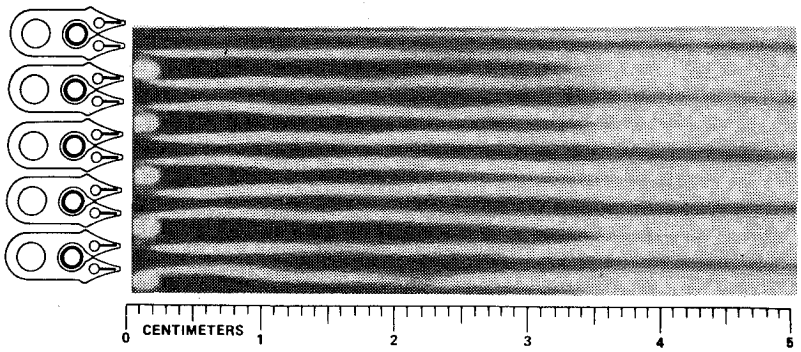

Fig. 7 HF cavity emission, $\mu = 0\%$ (0.10 g/s H_2 in secondary, trip-off).

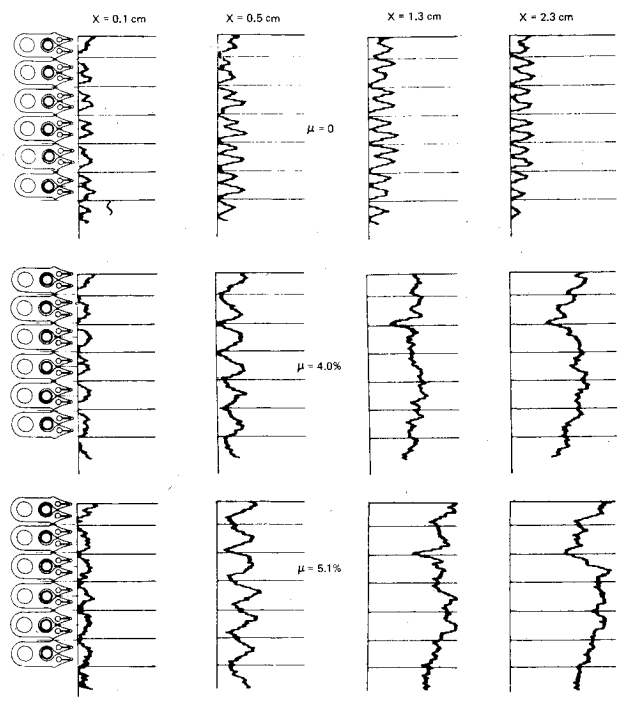

Fig. 8 Infrared scanner profiles of DF emission.

compete with D_2 for the atomic fluorine in the cavity; thus the HF emission intensity increases when the D_2 is absent.

Figure 7 shows the result when the jet flow is off and mixing occurs by laminar diffusion with no augmentation. It is clear from this photograph that the mixing characteristics of the laser with the jet flow off are fundamentally different from those when the jet flow is on. For this case, the HF emission occurs in a relatively narrow band which originates at the nozzle exit plane at the junction of the primary and secondary flows. This reaction zone gradually propagates into the primary flow and reaches the primary centerline at a downstream location greater than 5 cm, i.e., outside the field of view.

Infrared Scanner Tests

The infrared scanner was used to map the spontaneous emission in the 2-5 μm wavelength region. Tests were conducted at the $\dot{m}/A = 2.0$ g/s-cm^2 condition and at three levels of gas jet flow, i.e., $\mu = 0$, 4.0, and 5.1%. The relative intensity of the radiation as measured by the InSb detector is shown in Fig. 8. The intensity profiles are given for four axial locations as measured from the nozzle exit plane, i.e., 0.1, 0.5, 1.3, and 2.3 cm. Each intensity profile corresponds to a scan across the laser nozzle traversing six primary nozzles.

The results for the laminar mixing condition show a double-hump structure over the 0-2.3 cm range, with little or no

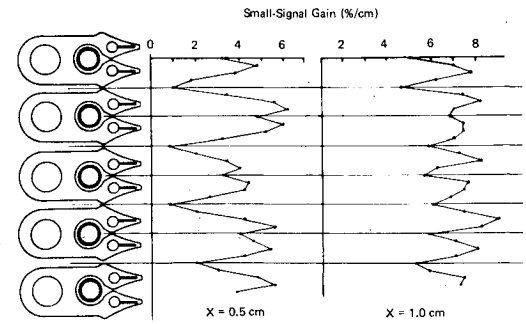

Fig. 9 Cross-nozzle small-signal gain P_2 (4) line, $\mu = 3\%$.

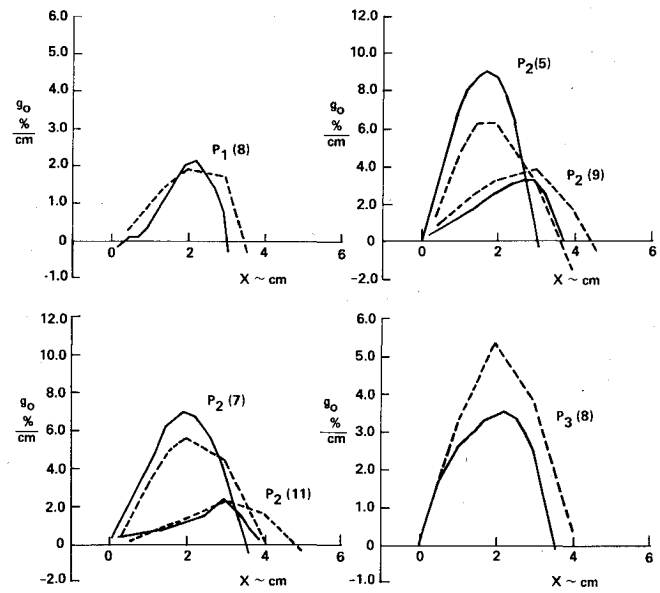

Fig. 10 Axial small-signal gain distributions, $\dot{m}/A = 20$, $\mu = 3\%$; data —, model – – –.

emission on the centerlines of the primary or secondary nozzles, and a sharply peaked emission region between these centerlines. The location of the intensity peak shows virtually no transverse movement over the 2.3 cm axial distance.

With regard to the intensity levels when $\mu > 0$, the results indicate that in the near-nozzle region ($x < 0.5$ cm), the peak emisson intensities are not very different from those for the laminar mixing case. For $x > 0.5$ cm, the emission intensity is higher than that for the laminar mixing condition and also, it has a different structure. Whereas the laminar mixing case maintains the sharply spiked structure over the 2.3 cm distance, the situation for the jet flow cases is quite different. At $x = 0.5$ cm, with the jet flow on, the highest emission intensity is on the centerline of the secondary nozzle flow; with

the jet flow off, there is little or no emission on the secondary centerline. At the $x=1.3$ and 2.3 cm locations with the jet flow on, the emission intensity profile has a more or less positive uniform value across the field of view, and at no point does the emission intensity drop to zero. Also note that the emission intensity is somewhat higher for the 5.1% trip flow test than for the 4% case.

Cross-Nozzle Small-Signal Gain Tests

Measurements were made of the cross-nozzle small-signal gain distributions for a number of DF lasing transitions. Figure 9 shows the cross-nozzle small-signal gain distributions for the $\dot{m}/A=2.0$ g/s-cm^2, $\mu=3\%$ test condition and the $P_2(4)$ transition. It is of interest to compare the structure of the gain distributions in Fig. 9 with the reaction zone structure shown in the photographs. Using Fig. 6 for comparison purposes, since it is the clearest of the photographs, the following similarities are noted. At the 0.5 cm axial location, Fig. 9 indicates a low ($\sim 1\%$) gain on the primary nozzle centerline; the photograph shows no chemical reaction at this location. In the neighborhood of the secondary nozzle centerline, the photograph shows a reacting shear layer with a lower reaction intensity on the centerline itself; Fig. 9 shows high gain in the secondary centerline region with a dip on the centerline. At the 1.0 cm location, the photograph indicates chemical reactions occurring across the entire nozzle; Fig. 9 shows a 7% average gain level at this location with the reacting shear layer structure still apparent. The similarity in the gain distributions and photographic reaction zone structures are quite close, especially when one recalls that the finite size of the laser probe beam tends to average the peaks of the gain distribution and the details of the photographic structure are sensitive to such parameters as exposure time and the film development process; both of these effects tend to obscure the comparison. A similar comparison for the laminar mixing trip-off test condition shows that the gain distributions are quite sharply peaked between the primary and secondary nozzle centerlines as would be expected from the photographic results in Fig. 7.

Interpretation

The objective of these experiments was to obtain information on the mixing characteristics of a chemical laser using the jet injection mechanism for mixing enhancement. Some care must be exercised in using photographic data for this purpose, in that the photographs record the emission zones of radiating species and these emission zones may or may not coincide with the fluid dynamic mixing boundaries. Before a specie can emit a photon, the cavity fuel must first mix with the oxidizer, then react to produce a molecule which can emit a photon in the spectral region in which the film emulsion is sensitive. Once the reactants are mixed, there are two characteristic times which influence the process, i.e., the reaction and spontaneous emission times. If these times are fast compared to the flow time, then the mixing and emission zone boundaries should coincide. As the reaction and emission times increase, then the emission zone boundaries will move downstream of the mixing zone boundaries. The emission zones, therefore, define the maximum downstream location of the mixing zone boundaries.

Radiation in the $\lambda \leq 1$ μm region, to which the infrared film is sensitive, is produced by HF and DF as it decays spontaneously from the upper vibrational levels by HF ($\Delta v \geq 3$) or DF ($\Delta v \geq 4$) transitions. When the fluorine atom and hydrogen mix, they react by way of the cold reaction, $H_2 + F \rightarrow HF(v) + H$, $v=1$-3. Therefore the primary reaction which occurs upon mixing, produces HF (3) which, by decay to HF (0), produces radiation in the wavelength region to which the film is sensitive. The characteristic reaction time is therefore that of the cold reaction. The situation is similar for lasers in which D_2 is the cavity fuel and DF (4) is the specie of interest [note that the cold reaction will pump DF(v) into the 4th vibrational level].

The characteristic time delay associated with the cold reaction can be estimated since the rate for this process is well known. If we consider a laser operating at 20 Torr cavity pressure with $T=300$ K and a stoichiometric mixture of fluorine atom and hydrogen, then the time required to produce an amount of HF (3) equal to 5% of the initial fluorine concentration is approximately 4×10^{-7} s. If the cavity flow velocity is approximately 2×10^5 cm/s, then the distance required to effect this conversion is 0.08 cm. Based on this, we conclude that the differences in the location of the mixing zone and emission zone boundaries due to the reaction time are likely to be small, on the order of 0.10 cm or less.

The IR scanner uses an LN_2-cooled InSb detector sensitive to radiation in the $\lambda=2$-5 μm region. The scanner therefore records the DF ($\Delta v=1$) radiation produced by the cold reaction. Due to the low detection threshold of the instrument, the IR scanner can detect and record the presence of DF(v) at very low concentration. It follows that the IR scanner should detect the presence of DF(v) somewhere within the 0.10 cm distance estimated for the rise of DF(v) from low to significant levels. Thus the IR scanner should detect the mixing boundaries within the accuracy associated with the characteristic distance of the cold reaction, i.e., 0.10 cm.

If the IR scanner will provide the most accurate definition of the mixing zone boundary locations, it then becomes possible to evaluate the accuracy of the photographic data by comparing it with that from the IR scanner. From the photographic data presented, it is clear that the photographs of the DF ($\Delta v \geq 4$) IR emission do not agree with the IR scanner results (compare Figs. 3 and 8) even qualitatively. On the other hand, the photographs of IR emission obtained using the H_2 seeding technique agree with the IR scanner data (compare Figs. 8 and 4-6) in detail with regard to the primary and secondary flow mixing zone boundaries for both the trip-on and laminar mixing cases.

The differences between the HF and DF photographic results can be explained by referring to the equation for total emission energy. Using HF(3) as an example, the energy emitted by HF(3) during time t at wavelength λ is $E=K(A_\lambda t/\lambda)$ [HF(3)] where A_λ is the transition probability (Einstein coefficient) for the λ transition under consideration, and K is a constant which depends on the experimental configuration. The ability to detect this concentration of HF(3) requires that E be greater than the minimum energy deposition required to expose the particular film being used. Interpreting t as the exposure time and noting that λ is about the same for DF ($\Delta v=4$) and HF ($\Delta v=3$), then for a fixed exposure time, $E \sim A_\lambda$. The transition probability, A_λ, for the DF ($\Delta v=4$) transition is approximately a factor of 200 smaller than that for the HF ($\Delta v=3$) transition. Thus, for the 5-10 s exposure times used in these experiments, while the light emission from the DF is insufficient to expose the film, the emission from HF, which is on the order of 10^2 times that from DF, provides very good definition.

While the arguments presented above are at best qualitative, they support the idea that the emission zones shown on the IR photographs using the hydrogen seeding technique provide a qualitative measure of the extent of mixing in the laser flowfield. The emission zone boundaries at least mark the maximum downstream location of the mixing boundaries, i.e., mixing must occur at a location either at or upstream of the emission zones. Thus, the photographs define the maximum primary and secondary flow mixing lengths.

Discussion

Hofland and Mirels[13] developed a laminar flame model for laser flows which indicates that for a fuel-rich mixture a thin

flame propagates into the oxidizer stream with the flame shape being given by $y_f \sim x^{1/2}$. The results in Fig. 7 show that the emission zone does indeed move into the oxidizer stream; however, the leading edge of the emission zone, which we take as marking the flame location, has a shape which is more nearly linear than parabolic. Since the emission zones in Fig. 7 mark the presence of the reaction products and provide no information about the oxidizer disappearance rate, these results cannot be used to judge whether or not a thin flame actually exists. The flame model contains many important simplifications; e.g., it neglects the nozzle boundary layers, oxidizer diffusion, and the influence of a finite fuel nozzle size, and thus one would not expect it to agree in detail with the Fig. 7 results. The differences between model and data, particularly with respect to flame shape, suggest however that the model be used for qualitative analyses only.

A number of important features are observed in the photographic data when the gas jets are used to disturb the flow. First, the axial mixing length decreases from the 5 cm laminar mixing value to values in the 0.5-1.0 cm range. Second, unlike the laminar mixing case, when the jet flow is on, the emission zone boundaries move from the nozzle lip into both the fuel and oxidizer streams. The emission zone boundaries are nearly linear with axial distance and the penetration angle is about 9 deg, i.e., $y_f \approx 0.15\,x$. Downstream of the 1 cm axial location, the IR scanner and gain results shown in Figs. 8 and 9 indicate a relatively uniform concentration of DF(v) in the cross-nozzle direction; this contrasts with the highly nonuniform distribution implied for the laminar mixing case by the results shown in Fig. 8.

Based on the results presented here, it is not possible to make a judgment as to the uniformity of the specie concentrations in the direction along the nozzle blade. The gain measurements shown in Fig. 9 are averaged along the 3.5 cm nozzle blade, and so too are the photographic and IR scanner data since these instruments record emission over finite field depth. One would suspect, however, that the flow is highly nonuniform along the nozzle blade since the gas jets have a large spacing/diameter ratio and thus will introduce a high degree of three-dimensionality into the flow. If the flow is nonuniform along the blade, then the photographs which indicate a fully mixed condition downstream of the 1 cm point should not be interpreted as implying the flow is homogeneous on a small scale downstream of this location. Rather, these photographs imply only that the convective processes induced by the gas jets have sufficient strength to transport reacting material to the nozzle centerlines over short axial distances. Further discussion of this aspect of the problem is given by Driscoll.[10]

While our understanding of the mixing augmentation mechanism induced by the gas jet injection is less than satisfactory, it is still possible to model this flow empirically. Figure 10 shows a comparison of the measured axial distribution of small-signal gain on six DF lines for the $\dot{m}/A = 2.0$ g/s-cm^2, $\mu = 3\%$ condition and the results calculated using the BLAZE-II computer code.[14] The agreement between data and theory is relatively good on all the lines in the three vibrational bands. For these calculations, the jet injection mixing augmentation was modeled by increasing the laminar diffusion coefficient by a factor of 2.5. The calculations indicate that the fuel and oxidizer streams are fully mixed at about 12 cm from the nozzle. If the 0.5 and 1.0 cm mixing lengths shown in the photographs are used to calculate the gain and laser power, then the model yields results which are about a factor of 2 higher than the data. This again suggests that the photographs should not be construed as implying that the flow is homogeneously mixed at the 1 cm location. The results also indicate a need for a model which properly accounts for the jet induced mixing mechanism.

Conclusions

In this paper we have demonstrated the utility of the hydrogen seeding technique as a means of photographically visualizing the reaction zones in a DF chemical laser. It was shown that the reaction zone structure indicated on the photograph is in agreement with that shown in the more quantitative IR scanner and small-signal gain mesasurements. The data clearly show the change in reaction zone structure which occurs when gas jet injection is used to increase the mixing rate. The photographic data indicate a factor of 5-10 reduction in the axial mixing length occurs when jet injection is used. The data also indicate that the jet induced mixing is not affected by the heat release level of the cavity flow. The short mixing lengths shown in the photographs cannot be predicted using the empirical mixing model which yields good agreement with the axial gain distributions. This suggests the flow is not homogeneously mixed at the 1 cm point where the photographs seem to indicate this is the case. Instead, the results imply the flow is probably highly nonuniform along the blade direction.

Acknowledgments

The work reported herein was supported by the U.S. Air Force under Contract F29601-77-C-0007. A number of people have contributed significantly to the work reported herein. The authors acknowledge with pleasure the contributions of R. E. Agthe, E. F. Clune, D. R. Janiak, W. Rickmond, W. L. Rushmore, C. E. Stricklin, R. Sutherland, and L. M. Wood.

References

[1] Mirels, H., Hofland, R., and King, W. S., "Simplified Model of CW Diffusion-Type Chemical Laser," *AIAA Journal*, Vol. 11, Feb. 1973, pp. 156-164.

[2] Broadwell, J. E., "Effect of Mixing Rate on HF Chemical Laser Performance," *Applied Optics*, Vol. 13, April 1974, pp. 962-967.

[3] Driscoll, R. J. and Moon, L. F., "Pressure Recovery in Chemical Lasers," *AIAA Journal*, Vol. 15, May 1977, pp. 665-673.

[4] Witte, A. B., et al., "Aerodynamic Reactive Flow Studies of the H_2/F_2 Laser-II," AFWAL-TR-74-78, Aug. 1974.

[5] Cummings, J. C., Hook, D. L., Witte, A. B., Shackleford, W. L., and Ackerman, R. A., "Use of a Fluid-Injector Trip Device to Enhance Cavity Mixing and Power of a DF Chemical Laser," *Proceedings of the First DoD Conference on High Energy Lasers*, Vol. I, Dec. 1974, pp. 541-554.

[6] Wilson, L. E. and Hook, D. L., "Deuterium Fluoride CW Chemical Laser," AIAA Paper 76-344, 1976.

[7] Shackleford, W. L., Witte, A. B., Broadwell, J. E., Trost, J. E., and Jacobs, T. A., "Experimental Studies of Chemically Reactive ($F+H_2$) Flow in Supersonic Free Jet Mixing Layers," AIAA Paper 73-640, 1973.

[8] Cenkner, A. A., "Laser Doppler Velocimeter Measurements on a Tripped DF Chemical Laser," *AIAA Journal*, Vol. 20, March 1982, pp. 383-389.

[9] Cenkner, A. A. and Driscoll, R. J., "Laser Induced Fluorescence Visualization on Supersonic Mixing Nozzles that Employ Gas-Trips," *AIAA Journal*, Vol. 20, June 1982, pp. 812-819.

[10] Driscoll, R. J., "The Effect of Reactant-Surface Stretching on Chemical Laser Performance," submitted to *AIAA Journal*.

[11] Yang, T. T., "Modeling of CW Chemical Laser with Annular Unstable Resonator," *AIAA Journal*, Vol. 18, Oct. 1980, pp. 1223-1232.

[12] O'Keefe, D., Sugimura, T., Behrens, W., Bullock, D., and Dee, D., "Comparison of LAMP and BLAZER Code Calculations with CL-XV Measurements," *Optical Engineering*, Vol. 18, July 1979, pp. 363-369.

[13] Hofland, R. and Mirels, H., "Flame-sheet Analysis of CW Diffusion-Type Chemical Lasers, I. Uncoupled Radiation," *AIAA Journal*, Vol. 10, April 1972, pp. 420-428.

[14] Zelazny, S. W., Driscoll, R. J., Raymonda, J. W., Blauer, J. A., and Solomon, W. C., "Modeling DF/HF CW Lasers: An Examination of Key Assumptions," *AIAA Journal*, Vol. 16, April 1979, pp. 297-304.